Available online at www.sciencedirect.com
SCIENCE DIRECT®
Agricultural and Forest Meteorology 119 (2003) 1–21
AGRICULTURAL AND FOREST METEOROLOGY
www.elsevier.com/locate/agrformet

Airflows and turbulent flux measurements in mountainous terrain Part 1. Canopy and local effects

Andrew A. Turnipseed[a,b,*], Dean E. Anderson[c], Peter D. Blanken[d], William M. Baugh[a], Russell K. Monson[a,e]

[a] *Department of Environmental, Population and Organismic Biology, University of Colorado, Boulder, CO 80309, USA*
[b] *Atmospheric Chemistry Division, National Center for Atmospheric Research, Boulder, CO 80305, USA*
[c] *US Geological Survey, Water Resources Division, Denver Federal Center, Lakewood, CO 80225, USA*
[d] *Department of Geography, University of Colorado, Boulder, CO 80309, USA*
[e] *Cooperative Institute for Research in Environmental Sciences (CIRES), University of Colorado, Boulder, CO 80309, USA*

Received 26 September 2002; received in revised form 13 May 2003; accepted 14 May 2003

Abstract

We have studied the effects of local topography and canopy structure on turbulent flux measurements at a site located in mountainous terrain within a subalpine, coniferous forest. Our primary aim was to determine whether the complex terrain of the site affects the accuracy of eddy flux measurements from a practical perspective. We observed displacement heights, roughness lengths, spectral peaks, turbulent length scales, and profiles of turbulent intensities that were comparable in magnitude and pattern to those reported for forest canopies in simpler terrain. We conclude that in many of these statistical measures, the local canopy exerts considerably more influence than does topographical complexity. Lack of vertical flux divergence and modeling suggests that the flux footprints for the site are within the standards acceptable for the application of flux statistics. We investigated three different methods of coordinate rotation: double rotation (DR), triple rotation (TR), and planar-fit rotation (PF). Significant variability in rotation angles at low wind speeds was encountered with the commonly used DR and TR methods, as opposed to the PF method, causing some overestimation of the fluxes. However, these differences in fluxes were small when applied to large datasets involving sensible heat and CO_2 fluxes. We observed evidence of frequent drainage flows near the ground during stable, stratified conditions at night. Concurrent with the appearance of these flows, we observed a positive bias in the mean vertical wind speed, presumably due to subtle topographic variations inducing a flow convergence below the measurement sensors. In the presence of such drainage flows, advection of scalars and non-zero bias in the mean vertical wind speed can complicate closure of the mass conservation budget at the site.

Keywords: Eddy covariance; Energy budget closure; Forest ecosystem; Complex topography; Drainage flows

1. Introduction

Micrometeorological methods for measuring the exchanges of heat, H_2O and CO_2 at the ecosystem level have been used with increased frequency in the past decade. Of the many micrometeorological methods, eddy covariance (EC) is considered the most reliable

* Corresponding author. Fax: +1-303-492-8699.
E-mail address: andrew.turnipseed@colorado.edu (A.A. Turnipseed).

0168-1923/$ – see front matter © 2003 Elsevier B.V. All rights reserved.
doi:10.1016/S0168-1923(03)00136-9

and accurate (Baldocchi et al., 1988; Aubinet et al., 2000), and its use has spawned a number of flux-measuring networks across the globe (Aubinet et al., 2000; Baldocchi et al., 2001). The EC method is not without its drawbacks. The theory that underlies this method relies on both spatial homogeneity and temporal stationarity (Kaimal and Finnigan, 1994; Foken and Wichura, 1996). However, these conditions are rarely, if ever, realized in natural ecosystems. Since the atmosphere is constantly changing, both spatial and temporal stationarity is only valid for short time periods (∼15–60 min). The presence of a tall plant canopy (Kaimal and Finnigan, 1994; Raupach, 1988) or sloping terrain (Jackson and Hunt, 1975; Taylor et al., 1987; Kaimal and Finnigan, 1994) adds complexity to the turbulence generated at the surface. Complexities in the surface terrain can lead to irregularities in the streamline flow and divergence in advective fluxes that are often neglected in the application of eddy covariance. Despite the difficulties and uncertainties caused by these complexities, recent work has shown that the EC approach does a reasonably accurate job of measuring surface fluxes in a variety of situations with complex terrain under suitable meteorological situations (Goulden et al., 1996; Baldocchi et al., 2000; Barford et al., 2001). Furthermore, re-evaluation of the mass conservation equation has led to new approaches, which address the complexities surrounding the horizontal and vertical components of the advective flux (Lee, 1998; Paw U et al., 2000). Although, not fully substantiated at present (Finnigan, 1999), these approaches appear promising at certain sites and should certainly be tested at other sites.

Turbulent fluxes from mountain ecosystems are critical to understand if we are to gain a realistic understanding of ecosystem-atmosphere carbon fluxes, and their relevance to modeling efforts that aim to quantify regional and global carbon budgets. In a recent modeling analysis, two biogeochemical models (Century and Biome-BGC) were used to assess regional carbon sequestration in the western US (Schimel et al., 2002). The models revealed that, depending on climatic conditions, up to 75% of the western US carbon sink occurs at elevations above 750 m, an elevation range dominated by hilly or mountainous topography. The pattern of carbon uptake illustrated that during periods of extended drought (e.g. decadal-scale drought during the 1980s), carbon sequestration by coastal forests is markedly suppressed, and regional foci of high carbon uptake occur in the Sierra Nevada and Rocky Mountains. When analyses of this type are combined with facts such that half the world's surface lies at elevations above 500 m, and mountain regions supply more than half the world's freshwater (Ives et al., 1997), it is crucial that we expend more effort and energy to study the complexities of making eddy flux measurements in mountainous terrain.

This paper is the first of two in which we discuss turbulent flux measurements in relation to complex terrain at the Niwot Ridge Ameriflux site (see Hollinger and Wofsy, 1997 for Ameriflux description). The study site lies on the leeward side of the Rocky Mountains of Colorado in a high-elevation, subalpine forest. Complications in mass and heat transport at the site arise due to both the presence of a forest canopy, as well as local and mesoscale topography. Despite these complexities, an evaluation of the surface energy budget has shown that closure of 84–88% is typical (Turnipseed et al., 2002). These results led us to conclude that EC measurements at the site represent the true surface fluxes as accurately as at other less topographically-challenged sites. However, there are few reported EC measurements within mountainous terrain (although see Banta, 1985; Geissbühler et al., 2000). Due to the suite of possible impacts on the local airflows induced by the canopy and topography, it is necessary to fully investigate the possible effects these complex flows have on turbulent flux measurements. In the first part of our series, we describe the impact of local effects, ranging from canopy structure to the local topography. In the second part of our series, we investigate the impacts of mesoscale topography and associated wind motions such as mountain waves, rotor winds and anabatic–katabatic winds.

2. Site description

The study was conducted at the Niwot Ridge Ameriflux site in the Roosevelt National Forest in the Rocky Mountains of Colorado (∼25 km west of Boulder, Colorado and ∼8 km east of the Continental Divide). The site is located at 40°1′58.4″N and 105°32′47.0″W on Arapahoe Moraine at an elevation of 3050 m. The terrain around the flux tower exhibits a slope of

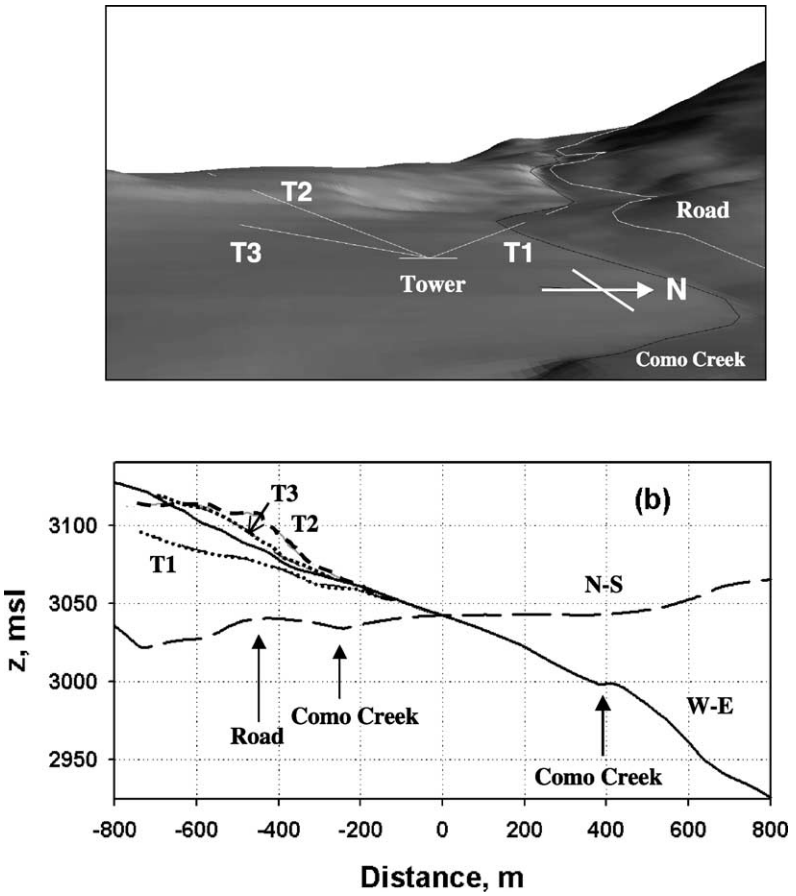

Fig. 1. (a) Digital elevation map of the Niwot Ridge Ameriflux site showing the tower and surrounding terrain. The vertical axis has been exaggerated by a factor of 3 to more clearly show topographical features. (b) Elevation changes along several transects for ±800 m surrounding the tower. Transects are shown for going: (i) west to east, (ii) north to south and the marked transects (T1 = 304°, T2 = 256° and T3 = 231°) shown in Fig. 1(a).

approximately 5–7° within 400 m in the east–west direction (Fig. 1). To the west, forested fetch continues for nearly 2 km along nearly flat or slightly sloping terrain. To the east, the fetch extends for approximately 400 m along a gentle slope (5–7°), before increasing to ∼10–13°. Approximately 5 km to the northwest of the tower, a large mountain peak influences regional flows. Directly north of the tower, this peak grades into a gentler uphill slope. Thus, the tower sits in an area characterized by the apparent convergence of downslope flows from the west, northwest and north.

The meteorology for the study area has been described in previous reports (Barry, 1973; Brazel and Brazel, 1983; Parrish et al., 1990; Turnipseed et al., 2002). The prevailing winds are from the west, flowing down the lee side of the Continental Divide. Summertime meteorology is typified by valley–mountain flows, with thermally-induced upslope flow from the east occurring on many afternoons (∼1/3 of the days). Upslope flow also occurs when synoptic storm systems pass to the south of the region or arctic fronts press into the area from the northeast; these events are often accompanied by precipitation. Nighttime flow is nearly always from the west, and is often katabatic (downslope drainage).

The forest surrounding the measurement tower is dominated by subalpine fir (*Abies lasiocarpa*), Engelmann spruce (*Picea engelmannii*) and lodgepole

pine (*Pinus contorta*). The average canopy height (h_c) is 11.4 m with an average stem density of 4000 stems ha^{-1}. The age of this secondary-growth forest is approximately 90 years. The canopy is relatively open with a leaf area index of $\sim 4.0\,m^2\,m^{-2}$ (one-sided seasonal maximum), and a gap fraction of ~17%.

3. Instrumentation and methods

Wind speeds at different heights along a 26 m tall scaffolding tower were measured with several types of anemometers. Table 1 provides a list of the types of anemometers and their measurement heights. Also included are results from intercomparisons of each type of sensor with a reference anemometer (CSAT-3, Campbell Scientific). Above 7 m ($z/h_c = 0.61$), anemometers were mounted on the main tower on horizontal booms extending ~1.8 m from the western edge of the tower. The booms were directed either northerly or southerly to avoid tower shadowing for both downslope (westerly) and upslope (easterly) flows. Below the canopy, anemometers were mounted on a 6 m tall triangular tower located in a forest gap approximately 20 m south of the main tower.

Continuous eddy covariance fluxes of sensible heat, momentum, H_2O, and CO_2 were measured at a height of 21.5 m ($z = 1.89h_c$). Detailed descriptions of these systems are provided in Turnipseed et al. (2002) and Monson et al. (2002). Table 1 includes a brief description of the sensor and corrections applied to the data. The Kr hygrometer was located within 36 cm of the sonic anemometer. Air for the closed-path IRGA was drawn from an inlet located 20 cm from the sonic anemometer path. The air was filtered and passed through a heat exchanger to reduce temperature fluctuations before analysis.

Table 1
Wind and flux instruments in the present study

z (m); z/h_c	Type of measurement	Sensor type	Footnotes
25.5; 2.24	Wind speed	Propvane	[a]
21.5; 1.89	Wind speed	3D sonic anemometer	[b]
	Sensible heat	3D sonic anemometer	[c]
	Latent heat	Kr hygrometer, IRGA	[d]
	CO_2 flux	IRGA	[e]
6.0–21.5; 0.53–1.89	Wind speed	3D sonic anemometer	[f]
	Sensible heat	3D sonic anemometer	
16.0; 1.40	Wind speed	Propvane	[a]
9.3; 0.79	Wind speed	2D sonic anemometer	[g]
6.5; 0.57	Wind speed	2D sonic anemometer	[g]
3.0; 0.26	Wind speed	3D sonic anemometer	[b]
	Sensible heat	3D sonic anemometer	
1.0; 0.09	Wind speed	3D sonic anemometer	[b]
	Sensible heat	3D sonic anemometer	

[a] RM Young, Model #090110. Wind speed and direction were compared against CSAT-3 3D sonic anemometer at 21.5 m. Wind speed regression: slope $= 0.996 \pm 0.004$, intercept $= -0.23$, $R^2 = 0.984$, $N = 3854$ in half-hour periods.

[b] CSAT-3, Campbell Scientific.

[c] Temperature covariance was corrected for humidity as described by Schotanus et al. (1983).

[d] Two systems: (1) open path Kr hygrometer (KH20, Campbell Scientific) and a closed-path infrared gas analyzer (Li-6262, LiCor, Inc.). Latent heat fluxes from the open path Kr hygrometer include corrections for oxygen absorption and density changes due to sensible heat flux (as described by Webb et al., 1980). No corrections were applied to the closed-path system.

[e] Li-6262 infrared gas analyzer (IRGA), LiCor, Inc. Corrections due to density changes caused by latent heat flux (Webb et al., 1980).

[f] ATI-K, Applied Technologies. Wind speed and flux intercomparisons made at $z = 21.5$ m ($z/h_c = 1.89$) for 2–4 months of data relative to a CSAT-3. Wind speed regression: slope $= 1.007 \pm 0.026$, intercept $= 0.024$, $R^2 = 0.989$, $N = 520$.

[g] Vaisala, Model #425A. Comparison made at $z = 2$ m ($z/h_c = 0.18$) for 6 weeks relative to a CSAT-3. Wind speed regression: slope $= 0.984 \pm 0.005$, intercept $= -0.06$, $R^2 = 0.97$, $N = 1300$ half-hour periods.

Signals from the CSAT sonic anemometers, Kr hygrometer and IRGA were digitized by dataloggers (CR23x, Campbell Scientific) at 10 Hz. Signals from all other sensors (propvanes, temperature, relative humidity, etc.) were also collected by dataloggers (CR23x, Campbell Scientific) at 1 s intervals. Data from these loggers and the ATI-K sonic anemometer were collected by a personal computer via RS-232 connections, synchronized in time, and then archived on a Sun workstation located in a trailer about 600 m from the tower.

Mean values and fluxes were calculated as a block average over an half-hour time period. Lag times between sensor signals and the vertical wind velocity (caused by transit time in the inlet tubing or by physical displacement of the sensor) were calculated by cross correlation between the respective scalar signal and the w wind velocity. Signals were shifted in time by this lag relative to w before covariances were calculated. Our typical protocol for flux calculation included mathematical rotation of the mean lateral ($\bar{v}$) and vertical ($\bar{w}$) wind velocities to zero following the procedure described by Kaimal and Finnigan (1994). (However, as discussed later, we have experimented with two other coordinate rotation methods to determine the best procedure for this complex site.) Only the lateral wind velocity was rotated in the derivation of under-canopy fluxes (Baldocchi and Hutchinson, 1987). Fluxes of sensible heat fluxes (H), latent heat (λE), and CO_2 were then calculated from the covariance between the vertical wind velocity temperature and the respective scalar as described by Webb et al. (1980). In addition to the flux sensors, we obtained data from a variety of meteorological sensors at the site, including those for mean values of radiation, temperature, humidity, precipitation; a complete listing of these and the measurement heights is given at http://public.ornl.gov/ameriflux/Participants/Sites/Site_Info/siteInfo.cfm.

4. Results and discussion

4.1. Footprint estimation

As an initial analysis of relevant flux footprints, and in an effort to better define what is meant by "local" fluxes, we employed the simple footprint model of Schuepp et al. (1990). Aubinet et al. (2000) report that the Schuepp model overestimates both the footprint peak distance and the cumulative footprint by about 20% compared to other widely used models (e.g. Horst and Weil, 1994; Wilson and Sawford, 1996). Thus, we consider this a conservative estimate of the footprint. Fig. 2(a) shows the footprint calculation for neutral atmospheric stability ($-0.1 < (z-d)/L < 0.1$), where d is the displacement height (see Section 4.2.1) and L the Obukhov length. Neutral conditions were typical during downslope westerly flow, especially during the winter (~70% of the time periods), and fetch calculation under these conditions yielded an upper limit to daytime flux footprints. After integrating the Schuepp footprint function, it was clear that >90% of the flux in the forest originated from within 1200 m of the tower. Since our western fetch is uniformly forested over that distance, it appears that fetch requirements were met in this wind direction for daytime fluxes.

However, our eastern fetch is not nearly as uniform; the slope changes significantly approximately 400 m east of the tower. Fortunately, near-neutral conditions are rarely observed for upslope flow (~3% of the time periods with easterly flow over the 3-year study period); typical conditions for upslope flow were high thermal instability and low wind speeds. These factors tend to shrink the calculated footprint (Fig. 2). As shown, the distance to the maximum flux contribution decreases from ~100 to ~50 m. Nearly 90% of the flux originated from distances of <500 m under typical upslope conditions. Although, we were working close to the bounds of our usable forest in the easterly direction, these calculations suggest that the majority of the flux was captured within the area just before the steep terrain for nearly all daytime periods.

Stable conditions often existed at night and they have a significant impact on the required fetch. With stabilities $[(z-d)/L]$ between 0.1 and 0.3, the 90% contribution limit expanded to beyond 3.5 km (data not shown). Under these conditions it is unlikely that adequate fetch exists at this site. However, this problem is common to most, if not all, eddy flux sites. High stability leads to decoupling of the airflows within and above the canopy. Even on relatively flat sites, turbulent fluxes measured above a canopy are not truly representative of the local surface flux under thermally stable conditions (Mahrt et al., 2000; Mahrt et al., 2001).

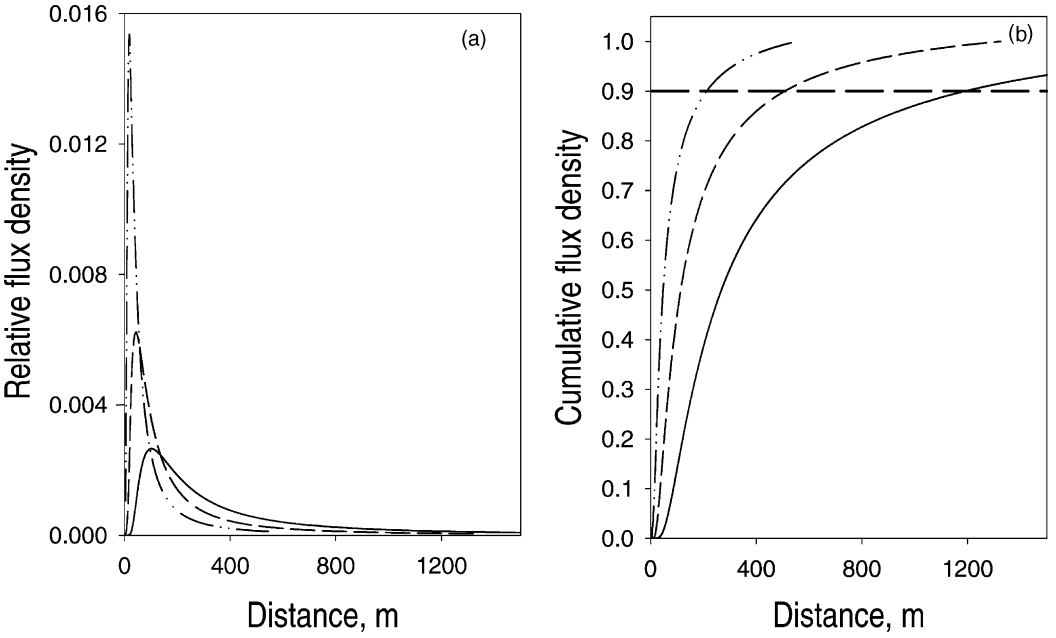

Fig. 2. (a) Relative flux density vs. linear upwind distance calculated using the model of Schuepp et al. (1990) at a flux measurement height of $z/h_c = 1.89$. Solid line is for neutral conditions ($(z-d)/L = -0.004$, $u^* = 1.6\,\mathrm{m\,s^{-1}}$, $U = 9.5\,\mathrm{m\,s^{-1}}$), dashed line is for unstable conditions ($(z-d)/L = -0.8$, $u^* = 0.38\,\mathrm{m\,s^{-1}}$, $U = 1.84\,\mathrm{m\,s^{-1}}$) typical of upslope conditions. Dot-dashed line is for same conditions but with a sampling height of $z/h_c = 1.18$. (b) Cumulative flux footprint vs. linear upwind distance for same conditions described in Fig. 2(a).

4.2. Vertical wind and turbulence structure

4.2.1. Displacement height and roughness length

The displacement height (d) and the roughness length (z_o) are two critical parameters needed to determine wind structure and momentum dissipation near the forest. Under near-neutral atmospheric stability ($-0.05 < z/L < 0.05$), the displacement height and roughness length can be derived from vertical wind speed profiles via:

$$U(z) = \frac{u^*}{k} \ln\left(\frac{z-d}{z_o}\right) \quad (1)$$

where z is the measurement height and k the von Karman constant (taken here as 0.4). In the fall of 1999, wind speed profiles at three heights (z/h_c = 1.18, 1.89 and 2.24) were combined with u^* values determined from the sonic anemometer (at $z/h_c = 1.89$) and fit to Eq. (1). However, as described by Wieringa (1993), values of d and z_o derived from such profiles are inversely correlated, and it is often difficult to determine the profile curvature (from whence d is derived) from only three levels. A further complication is that our lowest level is well within the roughness sublayer, which may cause the wind profile to vary from its expected logarithmic form. By looking at the derived d and z_o as a function of wind speed (data not shown), we noted that the two parameters became independent at high wind speeds ($U_{z=21.5} > 8\,\mathrm{m\,s^{-1}}$). We also noted that this wind regime was where intercomparisons of instruments exhibited best agreement (within ±2%, see Table 1). Upon applying this constraint, we determined $d = 7.8 \pm 1.1$ ($\sim 0.67 h_c$) and $z_o = 1.62 \pm 0.46$ ($\sim 0.14 h_c$) from 97 wind profiles. The value of $d = 0.67 h_c$ is not unexpected as the displacement height is typically found to be $\sim 0.75 h_c$ (Wieringa, 1993; Thom, 1971; Jackson, 1981). The value for z_o ($z_o = 0.15 h_c$) is larger than those expected in coniferous forests (typically $\sim 0.08 h_c$, Wieringa, 1993). The relatively large value of z_o is likely reflective of a relatively rough canopy with possible additional contributions from topographic roughness.

4.2.2. Turbulence intensity and skewness

We obtained an understanding of turbulence and wind field structure within the canopy by looking at

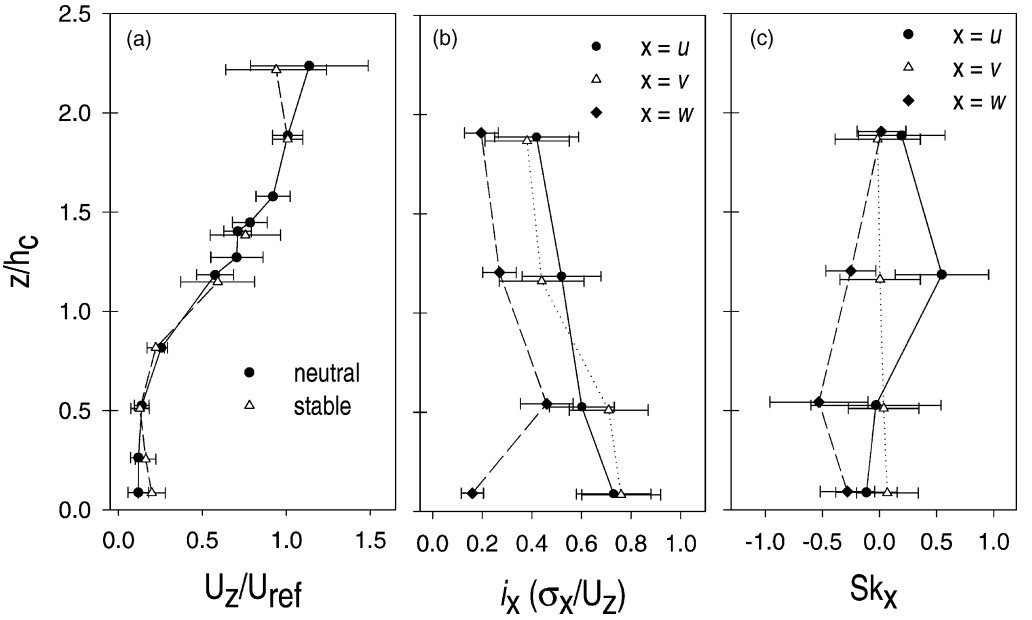

Fig. 3. Canopy profiles of: (a) normalized wind speed (where U_{ref} is U at $z/h_c = 1.89$) for both neutral and stable stratification. Points at $z/h_c = 1.89$ show the intercomparison between the ATI-K and the reference CSAT-3 anemometers (b) turbulent intensities (i_x) of u, v, and w, and (c) skewness (Sk) of u, v and w. Standard deviations from the mean are given by the error bars.

vertical profiles of wind speed, turbulence intensity and skewness in the wind velocity vectors (Fig. 3). Above the canopy, the familiar log-wind profile was observed (Fig. 3(a)). Descending into the canopy, wind speeds showed the characteristic inflection point near the canopy top (Raupach et al., 1996) and then decreased under neutral conditions. However, under stable conditions, a second maximum in wind speed was observed near the ground. This is most likely due to drainage flows as cold air sinks along the slope due to gravitational forcing.

Turbulence intensity was calculated as $i_x = \sigma_x/U_z$, where σ_x is the standard deviation of one of the wind components (u, v, or w) and U_z is the local mean wind speed. Maximum turbulence intensities reached values of $i_u \sim 0.6$–0.8 between $z/h_c = 0.09$–0.26, whereas i_w peaked at ~ 0.46 at $z/h_c = 0.53$. No seasonal differences were observed in turbulence intensity (Fig. 3(b)), even though average wind speeds and meteorological conditions were substantially different at different times of the year (Brazel and Brazel, 1983; Turnipseed et al., 2002). Turbulence intensities also showed no observable dependence on above-canopy atmospheric stability, wind direction or speed. Previous work in both deciduous (Baldocchi and Meyers, 1988a; Amiro, 1990a) and coniferous (Amiro, 1990a; Lee and Black, 1993) forest canopies has shown i_x maxima between $z = 0.5$–$0.8h_c$ for all these components, and generally our observed values fell within the range reported for these other canopies. Our observations showed a distinctive peak in i_w at $z \sim 0.5h_c$, but no similar features in i_u or i_v which, instead, showed peaks nearer to the ground. Near-ground maxima in i_u and i_v may, once again, have been due to drainage flows at the site.

Skewness (defined as the third statistical moment) describes the asymmetry of the probability density curve for a particular velocity component. Sk_u and Sk_w were typically near zero well above the canopy as is typical of the surface layer, becoming larger and diverging near the canopy top ($z/h_c = 1.18$, $Sk_u \sim 0.55$, $Sk_w \sim -0.25$, Fig. 3(c)). This pattern has been noted in several previous studies of forest canopies (Amiro, 1990a; Baldocchi and Hutchinson, 1987; Baldocchi and Meyers, 1988a) and implies the occurrence of large penetrating eddies as the largest source of mass transport within the canopy. It was the presence of these large, downward penetrating eddies

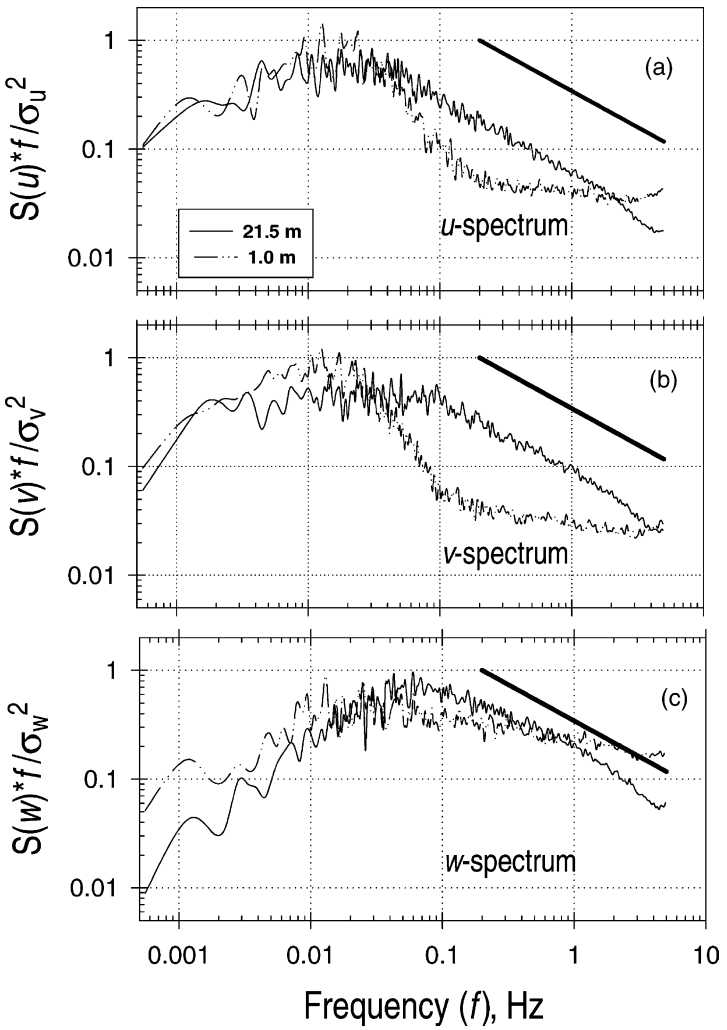

Fig. 4. Normalized power spectra of: (a) u, (b) v and (c) w at two different heights. Spectra are average of 10–14 half-hour periods during daytime with unstable atmospheric stability and moderate wind speeds ($\sim$4 m s^{-1}, $u^* = 0.3$–0.6 m s^{-1}). Solid line drawn is the expected $-2/3$ slope in the inertial subrange of the surface sublayer.

formed from shear at the top of the canopy that probably explains the maximum we observed in vertical turbulence intensity (i_w) at $z/h_c = 0.53$.

4.2.3. Characteristic time and length scales

When analyzed using spectral analysis, all wind velocities at $z = 21.5$ m ($z/h_c = 1.89$) followed the expected $-2/3$ power law (shown as the solid line in each plot) throughout the inertial subrange (Fig. 4). At 1.0 m, within the canopy trunk space, the power spectrum flattened out in the inertial subrange, indicating a spectral "shortcut", wherein drag on the tree boles and branches transfers energy directly from low to high frequencies (Kaimal and Finnigan, 1994). This spectral shortcut has been observed in several below-canopy studies (Shaw et al., 1974; Baldocchi and Meyers, 1988b; Amiro, 1990b; Meyers and Baldocchi, 1993; Blanken et al., 1998). Spectra at heights between these two extremes (data not shown) indicate that the spectral shortcut was observable only beneath the canopy ($z/h_c < 0.6$—no indication of shortcut at $z/h_c = 1.18$).

The natural frequency of the spectral peaks (f_m) for u and w were ~0.025 and 0.06 Hz at z = 21.5 m (z/h_c = 1.89), respectively (Fig. 4). These peaks varied little with height through the canopy (0.02–0.04 Hz for u, 0.03–0.06 Hz for w) similar to the study of Amiro (1990b) for three different canopies. The frequencies of the spectral peaks can be related to a length scale (assuming adherence to Taylor's theorem of "frozen turbulence") of the dominant energy-containing eddies by the local average wind speed ($\lambda = U_z/f_m$,). At z/h_c = 1.89, this yielded λ_u~170 m (14.7h_c, U_z~4.2 m s^{-1}) above the canopy. Beneath the canopy at z/h_c = 0.09, λ_u was found to be ~16 m (U_z = 0.32 m s^{-1}, f_m = 0.02 Hz) or 1.4h_c, still indicating the large size (~h_c) of eddies responsible for most of the transport at these heights.

The physical meaning of a length scale becomes problematic within canopies as Taylor's "frozen turbulence" hypothesis (which relates time-series statistics to spatial statistics) does not necessarily hold within the trunk space of canopies. This is because turbulent fluctuations can be larger than the mean wind speed (i.e. $i_x > 1$), thus causing the turbulent field to change in its statistical properties during the time it takes to advect an eddy past a fixed sensor (Kaimal and Finnigan, 1994; Amiro, 1990a). At our site, turbulent intensities (Fig. 3(b)) were, on average, less than unity throughout the canopy ($i_v \approx i_u \approx 0.75$ at z/h_c = 0.09), suggesting that Taylor's theorem may be applicable within the Niwot Ridge canopy. This may be due to the effect of the low LAI and openness of the Niwot Ridge canopy, which facilitates greater mean wind flow with less frequent interaction with canopy elements and, thus, lower turbulence intensities.

We used two indices to evaluate the persistence of local turbulence; the Eulerian length scale (Λ_x) as defined by a single-point statistical autocorrelation (Lenschow and Stankov, 1986), and the product (L_w) between the Eulerian time scale (T_w) and the standard deviation of w (σ_w) (i.e. $L_w = \sigma_w T_w$). Average values of Λ_u, Λ_v, Λ_w, and L_w showed no observable differences based on season, wind direction, u^* or U (data not shown). Values for Λ_w, Λ_u and Λ_v decreased steadily with decreasing height above the canopy (Fig. 5); this is in agreement with previous results (Amiro, 1990a; Kaimal and Finnigan, 1994) and reflects a decrease in eddy size as the canopy was approached. Within the surface layer, Λ_w was typically ~h_c and Λ_u was several times h_c (Raupach, 1988). This was consistent with our 21.5 m (z/h_c = 1.89)

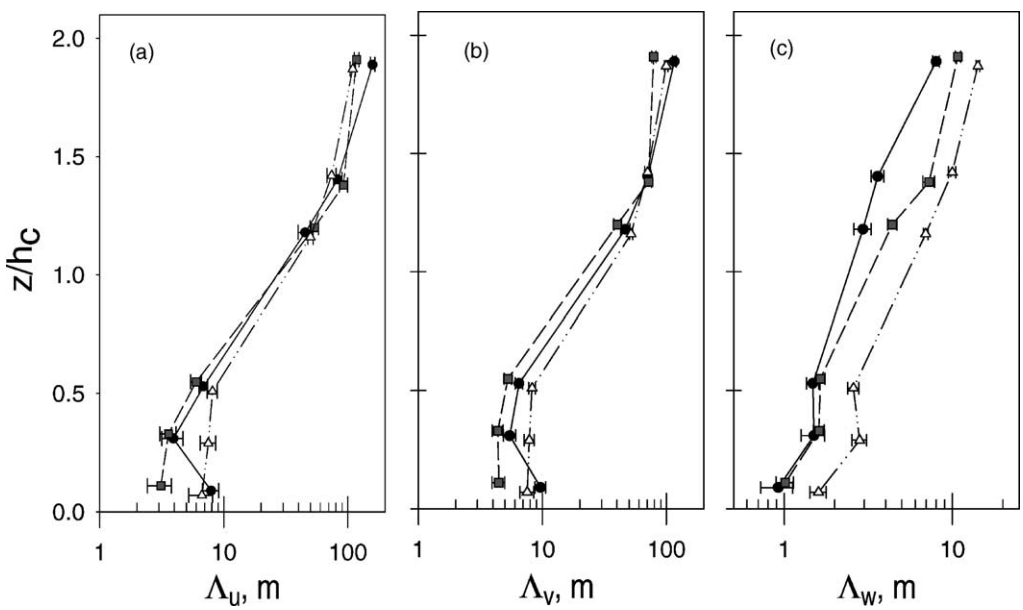

Fig. 5. Vertical profiles of Eulerian length scales (Λ_x) calculated for (a) u, (b) v, and (c) w. Symbols represent different above-canopy atmospheric stabilities: (●) stable, (■) neutral and (△) unstable conditions.

observations, whereby $\Lambda_w \sim 0.7$–$1.2h_c$ and $\Lambda_u \sim 9.6$–$14h_c$. L_w also decreased with height above the canopy in agreement with past studies (Baldocchi and Meyers, 1988b; Amiro, 1990a).

By looking at Λ_x as a function of above-canopy stability (Fig. 5), three notable observations emerged. (1) Unstable stratification consistently led to larger values for Λ_u, Λ_v and Λ_w relative to neutral conditions, presumably reflecting the larger turbulent scales associated with strong buoyant forcing. (2) At $z/h_c = 1.89$, Λ_u was significantly enhanced under stably stratified flows, which was not observed at $z/h_c = 1.18$. These observations suggest a possible decoupling between sheer-generated turbulence at the top of canopy and the airflow several meters above. (3) At the lowest height, a secondary maximum was observed for both Λ_u and Λ_v during stable above-canopy conditions. Faster wind speeds near the ground (see Fig. 3(a)) cannot be solely responsible for the maximum as no peak in Λ_w (which included U_z in its determination) was observed. It is likely that the presence of drainage flows near the ground increased horizontal transport under these conditions.

4.2.4. Vertical flux divergence

A second sonic anemometer (ATI-K) was positioned at various heights between $z/h_c = 1.18$ and 1.89, while maintaining a reference sonic anemometer (CSAT-3) at $z/h_c = 1.89$. Momentum and heat fluxes were recorded for periods of 2 weeks or longer at each height. All of the fluxes were included regardless of atmospheric stability. No evidence for significant vertical flux divergence was observed for either momentum or sensible heat fluxes (±4%, see Table 2). The lower u^* value obtained in the side-by-side comparison at $1.89z/h_c$ (6% difference between anemometers) was likely due to sensor shadowing; however, the sensible heat flux appeared unaffected. These observations imply the presence of a "constant flux layer" at our site, even throughout a substantial portion of the roughness sublayer (as least for sensible heat and momentum fluxes). We also observed no dependence of the sensible heat flux comparison between $z/h_c = 1.18$ and 1.89 on wind direction. Toward further analysis, recall that Fig. 2 also included a curve calculated for a sampling height of $z/h_c = 1.18$ under average upslope conditions. At this height, the footprint is considerably smaller than at the reference height of $z/h_c = 1.89$, such that 90% of the contribution to the measured flux occurs within ~225 m. This supports the conclusions drawn previously from the simple footprint calculations, that there is adequate fetch for turbulent flux measurements at $z/h_c = 1.89$ in both the primary wind directions (easterly upslopes and westerly downslopes) out to at least 500 m. Lack of vertical flux divergence also suggests that within the flux footprint and regardless of the heterogeneity of the vegetation, the flux measured at $z/h_c = 1.89$ (our reference height) is a reasonable measure of the actual surface flux.

4.2.5. Above-canopy integral turbulent statistics

The scaling of σ_w or σ_u by u^* provides valuable insight about the height of the roughness sublayer. Kaimal and Finnigan (1994) report that in the surface layer, $\sigma_w \sim 1.25u^*$ under neutral stratification and

Table 2
Comparison of temperature covariance ($w'T'$), friction velocity (u^*) and turbulent statistics (σ_w/u^*) measured at different heights

		21.5 m ($z/h_c = 1.89$)	18 m ($z/h_c = 1.58$)	16 m ($z/h_c = 1.40$)	14.5 m ($z/h_c = 1.27$)	13.5 m ($z/h_c = 1.18$)
N		519	605	507	397	1842
$w'T'$	Slope	1.062	1.043	1.043	1.043	1.085
	R^2	0.980	0.947	0.960	0.956	0.959
u^*	Slope	0.941	1.034	1.010	0.992	0.982
	R^2	0.955	0.986	0.954	0.935	0.940
σ_w/u^*		1.23–1.25	1.27	1.15	1.12	0.98

N = number of half-hour periods used in regression. All intercepts of the regressions were not significantly different than zero. The primary CSAT-3 sonic anemometer was maintained at $z = 21.5$ m and served as the independent variable in the above regressions. The secondary sonic anemometer (ATI-K) was mounted at the various heights listed above and faced in the same direction from the tower. σ_w/u^* values were obtained from plots of σ_w vs. u^* under near-neutral conditions ($-0.1 < (z-d)/L < 0.1$).

approaches $1.1u^*$ through the roughness sublayer, as the canopy is approached. For both summer and winter data from the Niwot Ridge site, σ_w/u^* was found to be 1.23 and 1.25, respectively, under neutral conditions at $z/h_c = 1.89$ (Table 2). As the canopy was approached (from $z/h_c = 1.40$ to 1.18), σ_w/u^* values decreased to near unity as expected. These results have led us to conclude that our primary measurement height at 21.5 m ($1.89h_c$) was above the roughness sublayer.

Since our measurement height appears to be within the surface layer, Monin–Obukhov similarity functions can be used to determine the reliability of flux data. Previous workers (Panofsky and Dutton, 1984; Foken and Wichura, 1996) have suggested using the scaled vertical velocity deviation (σ_w/u^*) as a means of validating flux data. Ideally, σ_w/u^* should obey an empirically-based turbulence model, which takes the form (Panofsky et al., 1977; Geissbühler et al., 2000):

$$\frac{\sigma_w}{u^*} = \alpha \left\{ 1 - \frac{\beta(z-d)}{L} \right\}^{\gamma} \quad (2)$$

where α, β and γ are empirically derived coefficients for different types of stability (neutral, stable and unstable) and z is the measurement height. Using the coefficients derived by Panofsky and Dutton (1984), the majority of the data from the Niwot Ridge site was adequately described by this model for $-4 < (z-d)/L \leq 0$, with approximately 10% of the time periods falling outside the ±30% criteria (Fig. 6). It appears that even over the complex terrain of our site, the surface layer scaling of σ_w with u^* behaves in a theoretically predictable fashion. With increasing stability [$(z-d)/L > 0$], agreement with the turbulence models was slightly less (data not shown), with ∼15% of the data falling outside the ±30% quality limits.

4.3. Effects of coordinate rotation

4.3.1. Effects on turbulent fluxes

The advantages of using a "streamline" coordinate system have been pointed out in several past reports (McMillen, 1988; Kaimal and Finnigan, 1994; Wilczak et al., 2001). Over complex terrain, such as gentle slopes or ridges, the streamline coordinate system can also be thought of as "terrain-following" coordinates (Wilczak et al., 2001). McMillen (1988) and Kaimal and Finnigan (1994) presented algorithms

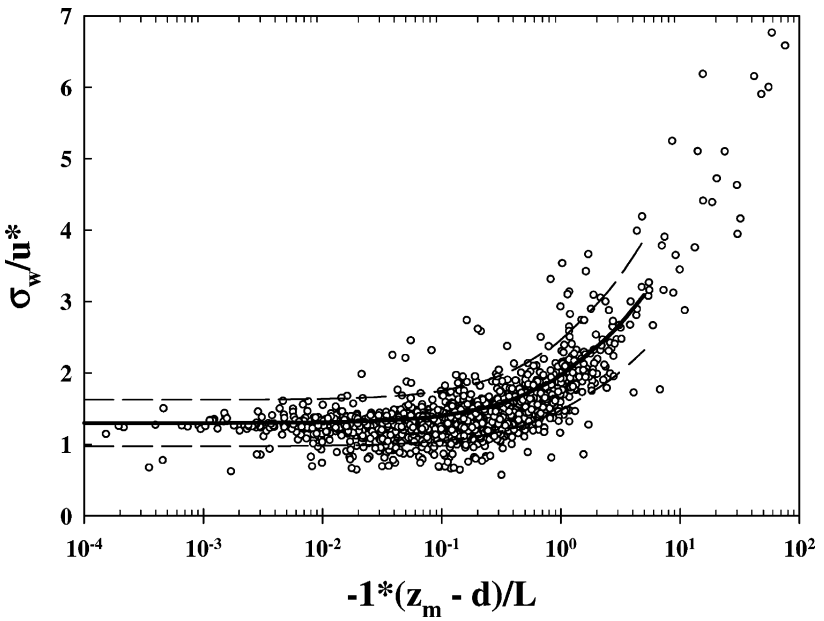

Fig. 6. Plot of σ_w/u^* vs. stability for near-neutral to unstable conditions at 21.5 m ($1.89h_c$). Data are for the summer of 2000. The solid line is the fit to Eq. (2) using the coefficients derived by Panofsky and Dutton (1984). The dashed lines are ±30%, which are recommended by Foken and Wichura (1996) as a criterion for data acceptance.

that could be used to rotate the 3D mean wind velocities into a coordinate system such that vertical velocities were normal to the mean flow.

In practice, coordinate rotation for each half-hour run is applied by sequentially forcing $\bar{v}$ (via angle θ_{uv}) and then $\bar{w}$ (via angle ϕ_{uw}) to zero (furthermore noted as double rotation (DR) method; McMillen, 1988; Kaimal and Finnigan, 1994). The triple rotation (TR) method is an extension of the DR method, where a third rotation is applied around the u-axis that forces $v'w' = 0$ (via angle ψ_{vw}). These two methods are the most prevalent means of coordinate rotation for flux stations participating in many of the current flux networks (Aubinet et al., 2000; Baldocchi et al., 2001).

A number of recent studies have re-ignited debate over the traditional coordinate rotation methods because of inadequate accommodation of advective fluxes (Lee, 1998; Finnigan, 1999; Baldocchi et al., 2000; Paw U et al., 2000; Lee and Hu, 2002) and contributions from low frequency fluxes (Sakai et al., 2001; Massman and Lee, 2002). Both the DR and TR methods contain the assumption that $\bar{w} \sim 0$ when averaged over a sufficiently long period which adheres to stationarity. This assumption has been questioned on the basis that: (1) advective components to the flux can, in fact, be significant (Lee, 1998; Lee and Hu, 2002; Massman and Lee, 2002), and (2) forcing $\bar{w}$ to zero is, in fact, a complicated high pass filter that can eliminate low frequency contributions to the flux (Massman and Lee, 2002). Wilczak et al. (2001) have also pointed out the implicit sampling errors in the DR or TR methods of rotation; errors that scale with the inverse of wind speed, thereby causing larger errors at low wind speeds.

Flux data from the Niwot Ridge site in the present and past (Turnipseed et al., 2002; Monson et al., 2002) studies were initially analyzed using the DR method. Rotation angles of ±5–8° were typical, in good agreement with estimates of the topographical slope obtained from maps (Fig. 7, Turnipseed et al., 2002). (By our notation, positive rotations are observed for downslope winds (clockwise rotation around the v-axis) and corresponding negative rotations for upslope winds.) Calculation of sensible heat, latent heat, and CO_2 fluxes without prior rotation led to (on average) 15–20% larger fluxes. Based on the typical atmospheric stabilities at Niwot Ridge, this error is in reasonable agreement with theoretical considerations (Wilczak et al., 2001).

A comparison of fluxes calculated by the DR and TR rotation methods for a subset of data (July 2000 and January 2001) revealed that agreement between the methods was excellent with derived slopes that were approximately unity (±0.02) (Figs. 8(a) and (c)). The average value of ψ_{vw} was small (∼2°), although we noted exceptionally large variations in ψ_{vw},

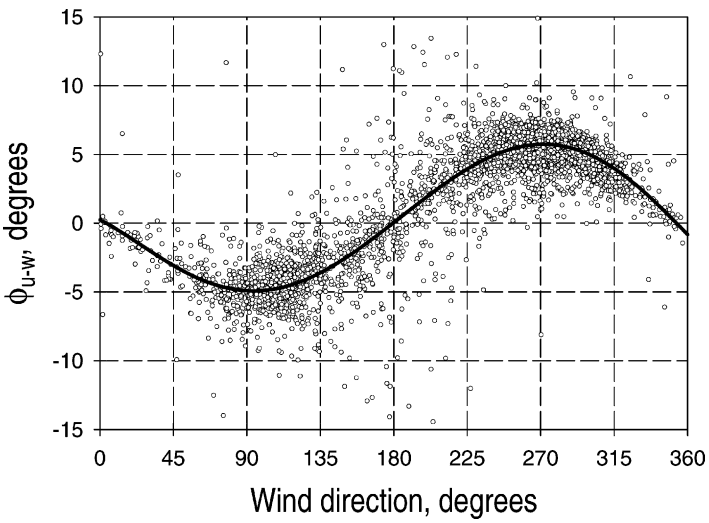

Fig. 7. Plot of rotation angle in the u–w plane (ϕ_{u-w}) vs. wind direction for July 2000 using the double rotation method (see text). Line drawn is a fifth-order polynomial fit to the data.

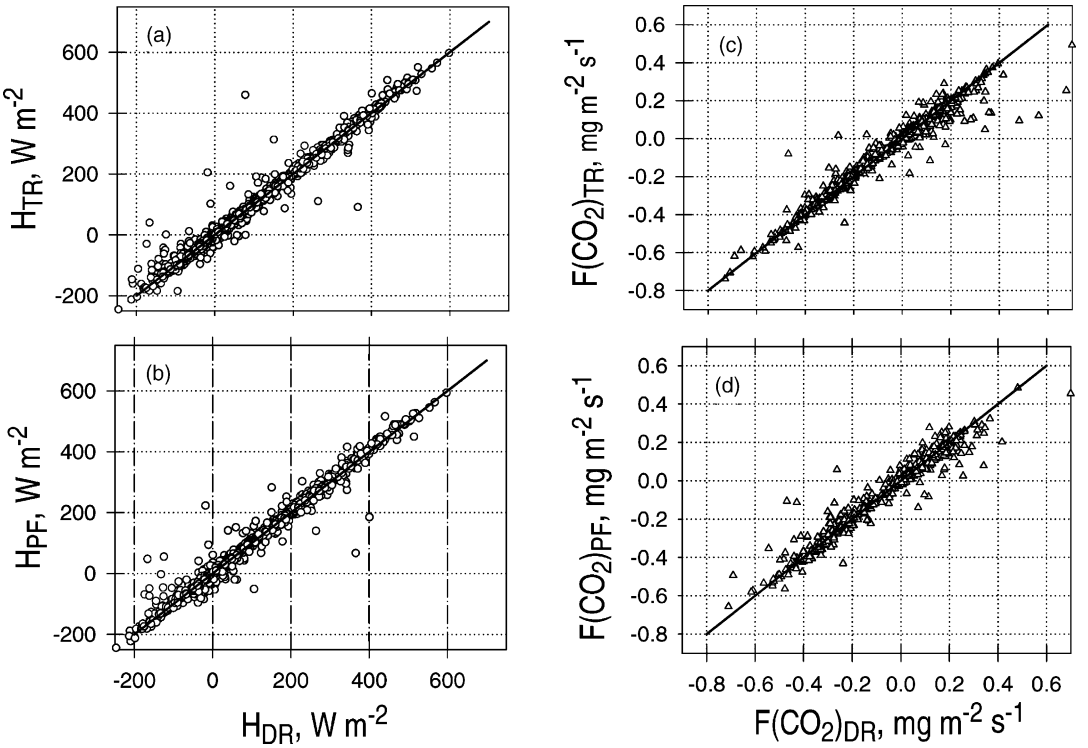

Fig. 8. Comparisons of the measured sensible heat (H) and $F(CO_2)$ for the triple rotation (subscripted TR—plots (a) and (c)) and the planar-fit (subscripted PF—plots (b) and (d)) methods relative to the double rotation method (subscript DR). Lines drawn are the 1:1 lines and linear regression fits to the data are not statistically different than 1.

ranging from near zero up to 10°. The variations were not consistent with the underlying topography and showed no systematic changes with other wind-related variables (e.g. wind speed and wind direction). Other studies have also noted that the inclusion of the third rotation can lead to large variability in derived covariances (Weber, 1999; Wilczak et al., 2001). Since, on average, the covariances were unaffected by the third rotation (Fig. 8), we conclude that substitution of the TR method for the DR method will not improve the analysis of fluxes at this site.

More recently, another method has been introduced that rotates the coordinate system to a best-fit plane that is parallel to the underlying topography (planar-fit (PF) method, Wilczak et al., 2001). This can be thought of as a "local long-term mean streamline flow" coordinate system (Finnigan, 1999). Within this method, measured mean vertical wind velocities, $\bar{w}_m$, for a given anemometer orientation, are regressed against the raw horizontal ($\bar{u}_m$) and cross-wind velocities ($\bar{v}_m$):

$$\bar{w}_m = b_0 + b_1\bar{u}_m + b_2\bar{v}_m. \quad (3)$$

The coefficients b_0, b_1 and b_2 are found by using multiple linear regression of a large set of measured velocities (averaged over 30 min periods). These coefficients are then used to determine rotation angles around the v-axis (α) and u-axis (β). When we applied this method to the Niwot Ride site, the angles derived from the regression of all the data were in good agreement with topographical measures (~5–6° along the east–west direction, ~2° along the north–south direction; Table 3). Although there was run-to-run variation (i.e. scatter around the slope), the slopes of the regressions of derived sensible heat and CO_2 fluxes obtained from the PF or DR method, were not statistically different from unity (Figs. 8(b) and (d)). Thus, with a large enough dataset, each method provided

Table 3
Planar-fit rotation angles derived at Niwot Ridge flux tower

Wind direction	U-range ($m\,s^{-1}$)	α°	β°	N (# points)	R^2
All	All	2.28 ± 0.03	5.32 ± 0.01	9659	0.97
West (220–325°)	All	2.54 ± 0.03	5.50 ± 0.01	7180	0.97
	<1.5	2.45 ± 0.22	4.31 ± 0.29	283	0.51
	1.5–3.0	2.94 ± 0.08	5.27 ± 0.09	1513	0.73
	3.0–5.0	2.57 ± 0.06	5.98 ± 0.09	2358	0.70
	5.0–7.0	2.53 ± 0.06	5.93 ± 0.13	1238	0.71
	7.0–9.0	2.50 ± 0.08	5.33 ± 0.21	734	0.70
	9.0–11.0	2.58 ± 0.11	5.47 ± 0.26	458	0.72
	>11.0	2.66 ± 0.15	5.68 ± 0.10	596	0.87
East (60–160°)	All	1.67 ± 0.07	4.19 ± 0.07	1996	0.66
	<1.0	1.10 ± 0.44	4.41 ± 0.61	153	0.26
	1.0–2.0	1.50 ± 0.15	4.52 ± 0.17	775	0.48
	2.0–3.0	1.58 ± 0.13	3.96 ± 0.14	757	0.53
	3.0–4.0	1.85 ± 0.14	4.23 ± 0.16	311	0.70

Errors are the standard error from the coefficients derived in the regression of Eq. (3).

the same average fluxes (also see Baldocchi et al., 2000; Wilczak et al., 2001).

Wilczak et al. (2001) noted that run-to-run variation of fluxes using the DR method should increase at low wind speeds due to sampling errors. This is amplified by the fact that highly variable wind directions during an half-hour period are often associated with low wind speeds and flows that have been in contact with variable terrain slopes (i.e. variable rotation angles) (Fig. 9(a)). At the Niwot Ridge site, as ϕ_{uw} is dependent on wind direction (Fig. 7), significant errors can potentially emerge in the flux data. To assess these effects, the data in Fig. 7 were fit to a fifth-order polynomial and residuals were calculated. At low wind speeds ($U < 3\,m\,s^{-1}$), ϕ_{uw} residuals tended to increase significantly (Fig. 9(b)). Errors in the computed tilt angle due to sampling errors in w can be estimated using the approach of Wilczak et al. (2001); at wind speeds of 1–2 $m\,s^{-1}$, we would expect tilt errors of ~3.4°. At the Niwot Ridge site, values of the residuals of ϕ_{uw} were often ±4–5° (Fig. 9(b)). This is slightly larger than the expected error, suggesting that errors in the calculated tilt angle also stemmed from other sources, such as wind direction variability. In contrast to the DR or TR methods, the planar-fit method does not suffer from errors due to the sampling of w, which might be particularly worrisome at low wind speeds. This was illustrated by the fact that $\bar{w}_z$ (defined as the mean vertical velocity for an half-hour period at measurement height z, after the planar-fit rotations have been applied), while being non-zero, showed little or no dependence on U (Fig. 9(c)). Looking at the percent differences between sensible heat fluxes (Fig. 9(d)) derived from the DR and PF methods gave a global average of 0.022 ± 0.006 (error is the standard error) with a nearly Gaussian distribution around the mean (Sk = 0.06), suggesting that the overall average fluxes were nearly identical for the two methods. However, particular periods can show large percent differences, most notably at low wind speeds. (It should be noted that periods of large percent differences often occur during periods of low flux—thus percentage differences can become larger.) During the periods of low wind speed ($U < 4\,m\,s^{-1}$), the average percent difference remained near zero (0.030 ± 0.007), but the distribution was positively skewed (Sk = 0.391). This suggests that the DR method caused some periods of flux overestimation relative to the planar-fit method under low wind speed conditions. This overestimation is further illustrated by looking at the integrated CO_2 flux for the dataset shown in Fig. 8. Over that time period, it was seen that the average daily integral of CO_2 flux was 3–5% less using the PF method as opposed to the DR method. In terms of long-term cumulative carbon uptake at the site, this effect is likely small, since the bi-directional nature of the CO_2 flux results in cancellation of the flux overestimation. However, it is an issue that deserves further scrutiny on annual data sets.

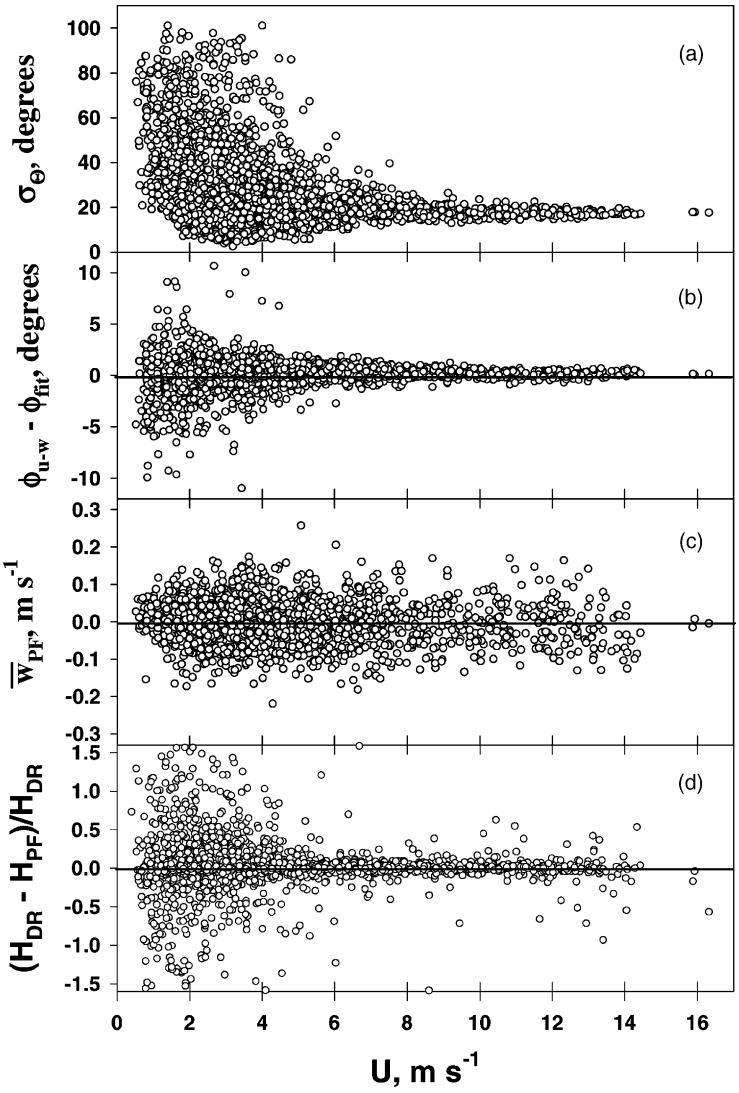

Fig. 9. Plots of: (a) the standard deviation of wind direction (σ_Θ), (b) the residual of the u–w transform angle (ϕ_{u-w}) relative to the best polynomial fit (in Fig. 7) and (c) $\bar{w}$ derived from the planar-fit (PF) method and (d) normalized difference in heat flux computed with the double rotation (DR) and planar-fit (PF) methods vs. wind speed (U).

4.3.2. Investigation of local flow patterns

Coordinate rotation also allows us to look at local flow patterns and characteristics by providing a reference frame relative to the underlying topography. On a constant slope with uniform flow, ϕ_{uw} from the DR method should exhibit a sinusoidal response with respect to wind direction (Paw U et al., 2000; Berger et al., 2001). A perfect sinusoid is not realized at the Niwot Ridge site, as the magnitude of ϕ_{uw} for easterly winds were typically less than what would be expected. To the east, even though the topographic slope increases beyond 400 m from the tower, the near-field inclination is relatively flatter than the slope immediately west of the tower (Fig. 1). Therefore, it appears that near-field topography is the major contributor to the calculated rotation angles. The PF was used to verify these observations by calculating rotation angles from different quadrants (Table 3). Smaller tilt angles

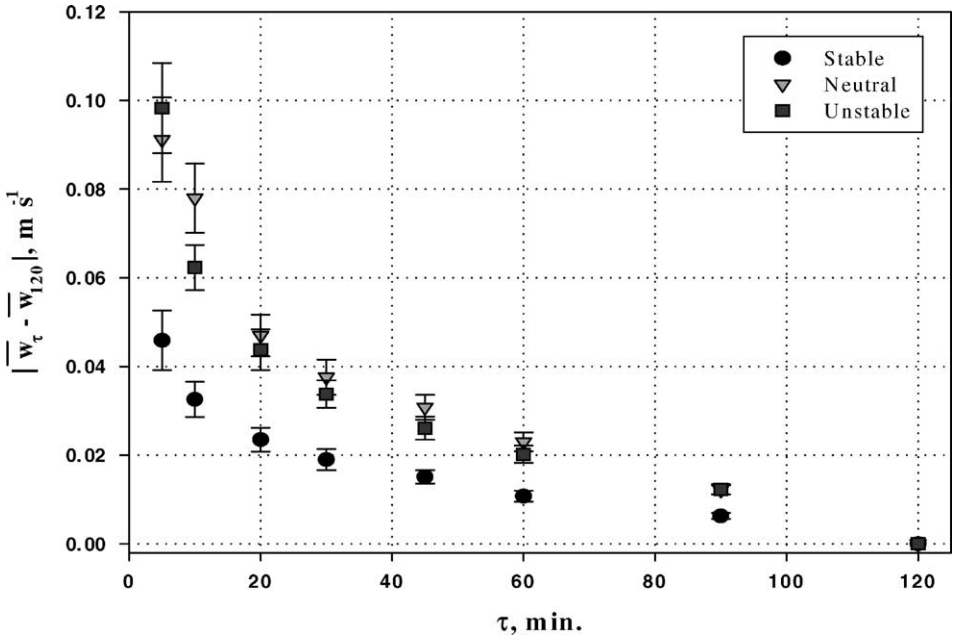

Fig. 10. Plot of the average $|\bar{w}_{(\tau)} - \bar{w}_{(120)}|$ vs. sample averaging time, τ, $\bar{w}_{(120)}$ is the mean vertical velocity over a 2 h (120 min) sampling interval and $\bar{w}_{(\tau)}$ the mean vertical velocity for the initial time interval, τ, contained within the larger 2 h sample period. Data are from 21–31 January and 21–31 July 2001. Raw 3D wind velocities were rotated using the planar-fit method before deriving $\bar{w}$ values.

were derived for easterly flow. No dependence of the PF angles upon wind speed was noted, suggesting that, on average, the local streamlines tended to follow the topography and possible streamline separation from the surface was minimal.

The PF rotation method provides a means to test if $\bar{w}$ truly approaches zero for a given averaging time over the complex topography of the Niwot Ridge site. Data from 22 days (11 days in January 2001 and 11 days in July 2001) at $z/h_c = 1.89$ were divided into 2 h time periods. Within each period, subrecords of the initial 5, 10, 20, 30, 45, 60 and 90 min were rotated via the PF method and $\bar{w}_z$ was calculated for each averaging time (τ); additionally, $\bar{w}_z$ was calculated for the entire 2 h time period [$\bar{w}_z(120)$]. When averaged for 2 h, $|\bar{w}_z(\tau) - \bar{w}_z(120)|$ approached zero (Fig. 10); but, even with the use of an 1 h averaging time (3600 s), average mean vertical velocities were still not equivalent to the 2 h mean (1–2 cm s^{-1} difference). This calls into question the assumption of $\bar{w} \sim 0$ over an half-hour averaging period made when using the DR method. More importantly, it shows the possible significance of either low frequency contributions to the flux (Sakai et al., 2001) and/or the presence of advective fluxes (Lee, 1998) to our local flux calculations. Previously, we investigated the first possibility by increasing the time over which the sensible or latent heat fluxes were averaged, and found that low frequency contributions were, in the range of ~4–6% (Turnipseed et al., 2002).

The contribution of advective fluxes to the overall flux is more difficult to quantify (Lee, 1998; Finnigan, 1999; Turnipseed et al., 2002; Massman and Lee, 2002). Lee (1998) re-examined the conservation equation for the surface flux of a scalar and, assuming no horizontal flux divergence or advection, derived a term for a vertical advective flux which varied with the mean vertical wind speed ($\bar{w}_z$). Lee (1998) described this as a mass flow component to the flux. The basic premise in this derivation provides that a negative $\bar{w}_z$ (subsidence) leads to a horizontal flow divergence below the measurement height and results in a loss of vertical turbulent flux. Conversely, a positive $\bar{w}_z$ should be indicative of flow convergence. In the initial Lee (1998) study, negative $\bar{w}_z$ values obtained at night over a deciduous forest under stable

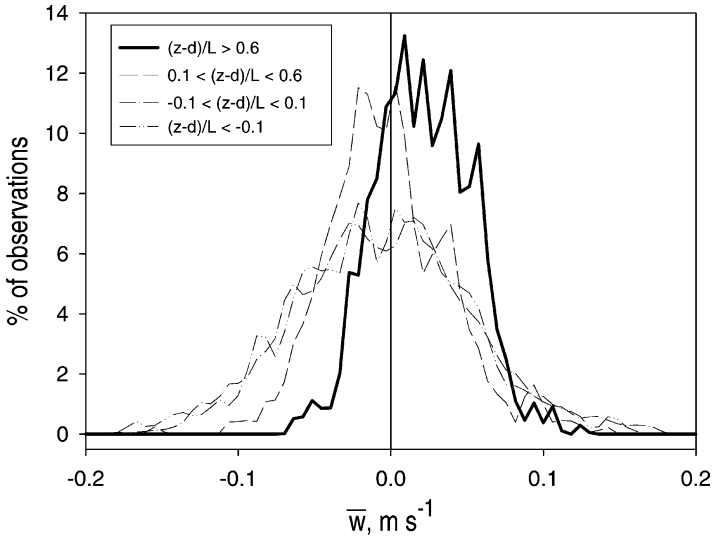

Fig. 11. Probability distribution of $\bar{w}$ (using $\tau = 1800$ s and for the same time periods as in Fig. 10) under varying atmospheric stabilities (denoted in the legend); $\bar{w}$ was derived after rotation using the planar-fit method.

stratification suggested a net drainage of air away from the base of the measurement tower, and he proposed that this could explain the loss of CO_2 flux observed under stable nocturnal periods.

In contrast to the Lee study, we often observed positive $\bar{w}_z$ values during nocturnal periods with low wind speeds and high atmospheric stability (Fig. 11). Under unstable, neutral and mildly stable stratification, the probability distribution of $\bar{w}_z$ was nearly symmetric about zero (mean $\bar{w}_z \leq \pm 0.007\,\mathrm{m\,s^{-1}}$). Conversely, under stronger stratification ($z/L > 0.6$), the distribution was skewed toward positive values (mean $\bar{w}_z = 0.021\,\mathrm{m\,s^{-1}}$), suggesting horizontal flow convergence beneath the tower. During these same periods: (1) wind speed profiles indicated that wind speeds at the forest floor ($z = 1$ m) exceeded those at mid-canopy ($z = 6$ m) (Figs. 3(c), 5, and 12), suggesting the presence of significant drainage flows near the ground, and (2) reduced turbulent fluxes of CO_2 (and large within-canopy CO_2 gradients) were observed (Fig. 12 and Monson et al., 2002).

Using these additional observations, the positive values of $\bar{w}_z$ during stably stratified periods are likely explainable by local changes in terrain and the effects of vegetation on the air flow path. As shown previously, directionally-derived rotation angles suggest a steeper slope to the west (and southwest) of the tower. The simple model of Mahrt (1982)

$$\bar{\bar{u}} = \left(\frac{g\bar{\bar{\theta}}}{\theta} X \sin \alpha_s \right)^{1/2}, \tag{4}$$

where g is gravitational acceleration, θ potential temperature, $\bar{\bar{\theta}}$ the average potential temperature depression in the flow, X the downslope distance and α_s is the slope angle, can be used to estimate the along-slope wind velocity ($\bar{\bar{u}}$) for gravity-driven drainage flow. In our case, this model predicted ~13% lower values for $\bar{\bar{u}}$ over a given distance, X, for a change in slope angle from 5.6° (to the west) to 4.1° (to the east). Additionally, more than one drainage channel for the below-canopy airflow could exist at our site (Fig. 1); the terrain is not unlike a small-scale mountain valley (Stull, 1988), where drainage flows originate along the sides (transects T2 and T3, Fig. 1(a)) and bottom (transects T1, Fig. 1(a)) of the valley. Thus, it is likely that advective flows tend to slow and converge within the vicinity of the flux tower. This phenomenon presumably causes air to accumulate and create a positive $\bar{w}_z$.

Alternatively, it is possible that forest structure explains the positive bias in $\bar{w}_z$. Our measurements of tree density have shown that within the 100 m fetch east of the tower, tree density, and concomitantly stem density, are significantly higher (data not shown). It is

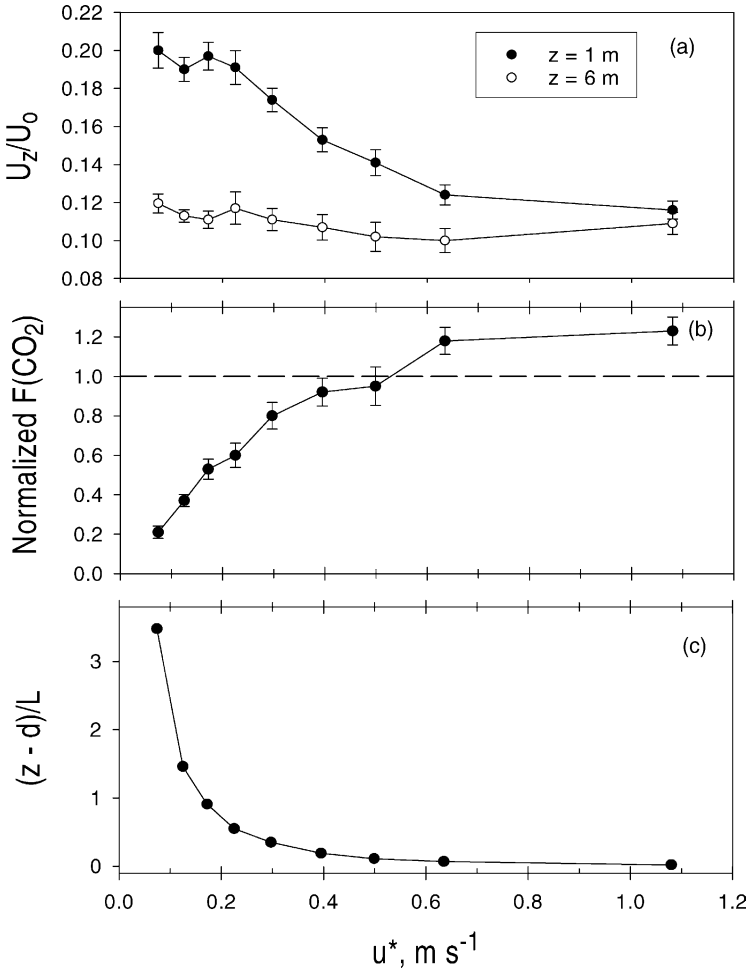

Fig. 12. Plots of: (a) normalized wind speed (with $U_o = U$ $(z/h_c = 1.89)$), (b) normalized CO_2 flux ($F(CO_2)$) and (c) stability $(z-d)/L$ as a function of friction velocity (both measured above the canopy) for nocturnal periods during the summer of 2001. Time periods were binned according to u^* and the points represent the average of these bins. Each bin contained between 230 and 456 half-hour time periods. $F(CO_2)$ was normalized by an "expected" flux generated by regressing the CO_2 fluxes vs. soil temperature during periods with $u^* > 0.25\,m\,s^{-1}$ (i.e. a u^* filter, see Goulden et al., 1996).

possible that increased wind drag on horizontal flows that proceed downhill, could slow the flow and force the upward movement of air at the tower. There is a clear need for further studies of this phenomenon at the Niwot Ridge site.

5. Conclusions

We have investigated numerous effects on local turbulent flux measurements at a site in mountainous terrain over a subalpine, coniferous forest canopy. Local canopy effects on turbulence were similar to those noted in many previous studies on simpler terrain, including the dominance of large penetrating gusts as the driving force for turbulent flux, spectral shortcuts in the transfer of turbulent kinetic energy, and vertical profiles of eddy length scales that showed decreases in eddy size as the canopy was approached. Although topography is complex, analysis of spectra and turbulent statistics suggested that turbulent eddy flux measurements during unstable to neutral atmospheric

stability could be made reliably. Three different methods of coordinate rotation were investigated and shown to give eddy fluxes that were in excellent agreement. No significant differences in fluxes were noted among the methods; however, in agreement with Wilczak et al. (2001), larger variability in rotation angles at low wind speeds were encountered with the commonly used double (DR) and triple (TR) rotation methods. This tended to cause flux calculations for some periods to be overestimated using the conventional DR method. Analysis of the residual mean vertical velocity using the PF method suggested that averaging times longer than a half-hour may be necessary to fulfill the requirement that $\bar{w} \sim 0$, implicit in the DR and TR methods, although errors associated with the half-hour averaging time may be relatively small.

The planar-fit method was also shown to be valuable in evaluating flow patterns encountered in complex topography, providing a reference frame similar to that of gravity over flat terrain. This was used to show that the flow patterns at the measurement tower changed with the local topographic slope. The unequal channeling of flows near the ground, along with frequent drainage flows at the site, are likely to cause two potential problems that need further study: (1) a positive bias in $\bar{w}$, and (2) advective scalar fluxes. Further research at the site will focus on the frequency of these effects and their quantitative contribution to the determination of cumulative turbulent fluxes.

Acknowledgements

The authors would like to thank the other members of the Monson research group for their assistance and contributions. Dr. Jed Sparks and Kim Sparks provided much of the biometric data. Dr. Dave Bowling provided invaluable help in establishing the flux systems during early stages of the project. The authors would also like to thank members of the Atmospheric Technology Division of the National Center for Atmospheric Research for assistance and guidance in establishing this research site and the data acquisition system. Special thanks are offered to Dr. Tony Delany, Gordon McLean, and Dr. Steve Oncley for their time and efforts. The authors would also like to thank Dr. Bill Bowman and staff at the University of Colorado Mountain Research Station and the Niwot Ridge Long-Term Ecological Research (LTER) site. Finally, we would like to thank the US Forest Service for permitting the establishment of the research site in the Roosevelt National Forest. This research was funded by the South Central Section of the National Institute for Global Environmental Change (NIGEC) through the US Department of Energy (DOE) (Cooperative Agreement No. DE-FC03-90ER61010) and a DOE Grant (DE-FG03-00ER63025) from the Terrestrial Carbon Processes (TCP) program. Any opinions, findings, and conclusions or recommendations expressed in this publication are those of the authors and do not necessarily reflect the views of the DOE.

References

Amiro, B.D., 1990a. Comparison of turbulence statistics within three boreal forest canopies. Boundary Layer Meteorol. 51, 99–121.

Amiro, B.D., 1990b. Drag coefficients and turbulence spectra within three boreal forests canopies. Boundary Layer Meteorol. 52, 227–246.

Aubinet, M., Grelle, A., Ibrom, A., Rannik, U., Moncrieff, J., Foken, Th., et al., 2000. Estimates of the annual net carbon and water exchanges of european forests: the EUROFLUX methodology. Adv. Ecol. Res. 30, 113–174.

Baldocchi, D.D., Hutchinson, B.A., 1987. Turbulence in an Almond Orchard: vertical variations on turbulent statistics. Boundary Layer Meteorol. 40, 127–146.

Baldocchi, D.D., Meyers, T.P., 1988a. Turbulence structure in a deciduous forest. Boundary Layer Meteorol. 43, 345–364.

Baldocchi, D.D., Meyers, T.P., 1988b. A spectral and lag correlation analysis of turbulence in a deciduous forest canopy. Boundary Layer Meteorol. 45, 31–58.

Baldocchi, D.D., Hicks, B.B., Meyers, T.P., 1988. Measuring biosphere–atmosphere exchanges of biologically related gases with micrometeorological methods. Ecology 69, 1331–1340.

Baldocchi, D.D., Finnigan, J., Wilson, K., Paw U, K.T., Falge, E., 2000. On measuring net ecosystem carbon exchange over tall vegetation on complex terrain. Boundary Layer Meteorol. 96, 257–291.

Baldocchi, D.D., Falge, E., Gu, L., Olson, R., Hollinger, D., Running, S., et al., 2001. Bull. Am. Meteorol. Soc. 82, 2415–2434.

Banta, R.M., 1985. Late-morning jump in TKE in the mixed layer over a mountain basin. J. Atmos. Sci. 42, 407–411.

Barford, C.C., Wofsy, S.C., Goulden, M.L., Munger, J.W., Pyle, E.H., Urbanski, S.P., et al., 2001. Factors controlling long- and short-term sequestration of atmospheric CO_2 in a mid-lattitude forest. Science 294, 1688–1691.

Barry, R.G., 1973. A climatological transect on the east slope of the front range, Colorado. Arct. Alp. Res. 5, 89–110.

Berger, B.W., Davis, K.J., Yi, C., Bakwin, P.S., Zhao, C.L., 2001. Long-term carbon dioxide fluxes from a very tall tower in a northern forest: flux measurement methodology. J. Ocean. Atmos. Technol. 18, 529–542.

Blanken, P.D., Black, T.A., Neumann, H.H., den Hartog, G., Yang, P.C., Nesic, Z., et al., 1998. Turbulent flux measurements above and below the overstory of a boreal aspen forest. Boundary Layer Meteorol. 89, 109–140.

Brazel, A., Brazel, P., 1983. Summer diurnal wind patterns at Niwot Ridge, CO. Phys. Geog. 4, 53–61.

Finnigan, J.J., 1999. On micrometeorological observations of surface-air exchange over tall vegetation (A comment on the paper by Lee (1998)). Agric. For. Meteorol. 97, 55–64.

Foken, Th., Wichura, B., 1996. Tools for the quality assessment of surface-based flux measurements. Agric. For. Meteorol. 78, 83–105.

Geissbühler, P., Siegwolf, R., Eugster, W., 2000. Eddy covariance measurements on mountain slopes: the advantage of surface-normal sensor orientation over a vertical set-up. Boundary Layer Meteorol. 96, 371–392.

Goulden, M.J., Munger, J.W., Fan, S.-M., Daube, B.C., Wofsy, S.C., 1996. Measurement of carbon sequestration by long-term eddy covariance: methods and critical evaluation of accuracy. Global Change Biol. 22, 169–182.

Hollinger, D.Y., Wofsy, S.C., 1997. Science Plan for AmeriFlux: Long-term Flux Measurement Network of the Americas, http//www.esd.ornl.gov/programs/NIGEC/scif.html.

Horst, T.W., Weil, J.C., 1994. How far is far enough? The fetch requirements for micrometeorological measurement of surface fluxes. J. Ocean. Atmos. Technol. 11, 1018–1025.

Ives, J.D., Messerli, B., Spiess, E., 1997. Mountains of the World—a global priority. In: Messerli, B., Ives, J.D. (Eds.), Mountains of the World—A Global Priority, Parthenon Publishing Group, New York, pp. 1–15.

Jackson, P.S., 1981. On the displacement height in the logarithmic velocity profile. J. Fluid Mech. 111, 15–25.

Jackson, P.S., Hunt, J.C.R., 1975. Turbulent wind flow over a low hill. Quart. J. Roy. Meteor. Soc. 101, 929–955.

Kaimal, J.C., Finnigan, J.J., 1994. Atmospheric Boundary Layer Flows: Their Structure and Measurement, Oxford University Press, Oxford.

Lee, X., 1998. On micrometeorological observations of surface-air exchange over tall vegetation. Agric. For. Meteorol. 91, 39–49.

Lee, X., Black, T.A., 1993. Atmospheric turbulence within and above a Douglas-fir Stand. Part I: Statistical properties of the velocity field. Boundary Layer Meteorol. 64, 149–174.

Lee, X., Hu, X., 2002. Forest-air fluxes of carbon, water and energy over non-flat terrain. Boundary Layer Meteorol. 103, 277–301.

Lenschow, D.H., Stankov, B.B., 1986. Length scales in the convective boundary layer. J. Atmos. Sci. 43, 1198–1209.

Mahrt, L., 1982. Momentum balance of gravity flows. J. Atmos. Sci. 39, 2701–2711.

Mahrt, L., Lee, X., Black, A., Neumann, H., Staebler, R.M., 2000. Nocturnal mixing in a forest subcanopy. Agric. For. Meteorol. 101, 67–78.

Mahrt, L., Vickers, D., Nakamura, R., Soler, M.R., Sun, J., Burns, S., et al., 2001. Shallow drainage flows. Boundary Layer Meteorol. 101, 243–260.

Massman, W.J., Lee, X., 2002. Eddy covariance flux corrections and uncertainties in long-term studies of carbon and energy exchanges. Agric. For. Meteorol. 113, 121–144.

McMillen, R.T., 1988. An eddy correlation technique with extended applicability to non-simple terrain. Boundary Layer Meteorol. 43, 231–245.

Meyers, T.P., Baldocchi, D.D., 1993. Trace gas exchange above the floor of a deciduous forest. Part 2: SO_2 and O_3 deposition. J. Geophys. Res. 98, 12631–12638.

Monson, R.K., Turnipseed, A.A., Sparks, J.P., Harley, P.C., Scott-Denton, L.E., Sparks, K., et al., 2002. Carbon sequestration in a high-elevation subalpine forest. Global Change Biol. 8, 1–20.

Panofsky, H.A., Dutton, J.A., 1984. Atmospheric Turbulence, Wiley, New York.

Panofsky, H.A., Tennekes, H., Lenshow, D.H., Wyngaard, J.C., 1977. The characteristics of turbulent velocity components in the surface layer under convective conditions. Boundary Layer Meteorol. 11, 355–361.

Parrish, D.D., Hahn, C.H., Fahey, D.W., Williams, E.J., Bollinger, M.J., Hubler, G., et al., 1990. Systematic variations in the concentrations of NO_x (NO Plus NO_2) at Niwot Ridge, Colorado. J. Geophys. Res. 95, 1817–1836.

Paw U, K.T., Baldocchi, D.D., Meyers, T.P., Wilson, K.B., 2000. Correction of eddy-covariance measurements incorporating both advective effects and density fluxes. Boundary Layer Meteorol. 97, 487–511.

Raupach, M.R., 1988. Canopy transport processes. In: Steffen, W.L., Denmead, O.T. (Eds.), Flow and Transport in the Natural Environment: Advances and Applications, Springer–Verlag, Berlin, pp. 95–127.

Raupach, M.R., Finnigan, J.J., Brunet, Y., 1996. Coherent eddies and turbulence in vegetation canopies: the mixing-layer analogy. Boundary Layer Meteorol. 78, 351–382.

Sakai, R.K., Fitzjarrald, D.R., Moore, K.E., 2001. Importance of low-frequency contributions to eddy fluxes observed over rough surfaces. J. Appl. Meteorol. 40, 2178–2192.

Schimel, D., Kittel, T., Running, S., Monson, R., Turnipseed, A., Anderson, D., 2002. Carbon sequestration studied in Western US mountains, EOS transaction. Am. Geophys. Union 83, 445.

Schotanus, P., Nieuwstadt, F.T.M., De Bruin, H.A.R., 1983. Temperature measurement with a sonic anemometer and its application to heat and moisture fluxes. Boundary Layer Meteorol. 26, 81–93.

Schuepp, P.H., Leclerc, M.Y., MacPherson, J.I., Desjardins, R.L., 1990. Footprint prediction of scalar fluxes from analytical solutions of the diffusion equation. Boundary Layer Meteorol. 50, 355–373.

Shaw, R.H., Silversides, R.H., Thurtell, G.W., 1974. Some observations of turbulence and turbulent transport within and above plant canopies. Boundary Layer Meteorol. 5, 429–449.

Stull, R.B., 1988. An Introduction to Boundary Layer Meteorology, Kluwer Academic Publishers, Dordrecht.

Taylor, P.A., Mason, P.J., Bradley, E.F., 1987. Boundary layer flow over low hills. Boundary Layer Meteorol. 39, 107–132.

Thom, A.S., 1971. Momentum absorption by vegetation. Quart. J. Roy. Meteorol. Soc. 97, 414–428.

Turnipseed, A.A., Blanken, P.D., Anderson, D.E., Monson, R.K., 2002. Surface energy balance above a high-elevation subalpine forest. Agric. For. Meteorol. 110, 177–201.

Webb, E.K., Pearman, G.I., Leuning, R., 1980. Correction of flux measurements for density effects due to heat and water vapor transfer. Quart. J. Roy. Meteorol. Soc. 106, 85–100.

Weber, R.O., 1999. Remarks on the definition and estimation of friction velocity. Boundary Layer Meteorol. 93, 197–209.

Wieringa, J., 1993. Representative roughness parameters for homogeneous terrain. Boundary Layer Meteorol. 63, 323–363.

Wilczak, J.M., Oncley, S.P., Stage, S.A., 2001. Sonic anemometer tilt correction algorithms. Boundary Layer Meteorol. 99, 127–150.

Wilson, J.D., Sawford, B.L., 1996. Review of Lagrangian stochastic models for trajectories in the turbulent atmosphere. Boundary Layer Meteorol. 78, 191–210.